



Cite this: *Chem. Commun.*, 2024, 60, 5213

Received 7th February 2024,  
Accepted 15th April 2024

DOI: 10.1039/d4cc00656a

rsc.li/chemcomm

## Tuning the redox profile of the 6,6'-biazulenic platform through functionalization along its molecular axis<sup>†</sup>

Shaun R. Kelsey, <sup>a</sup> Georgii Griaznov, <sup>a</sup> Andrew D. Spaeth, <sup>a</sup> Daron E. Janzen, <sup>b</sup> Justin T. Douglas, <sup>c</sup> Ward H. Thompson <sup>a</sup> and Mikhail V. Barybin <sup>\*a</sup>

**The  $E_{1/2}$  potential associated with reduction of the linearly-functionalized 6,6'-biazulenic scaffold is accurately correlated to the combined  $\sigma_p$  Hammett parameters of the substituents over  $>600$  mV range. X-ray crystallographic analysis of the 2,2'-dichloro-substituted derivative revealed unexpectedly short C–Cl bond distances, along with other metric changes, suggesting a non-trivial cycloheptafulvalene-like structural contribution.**

Originally isolated from plant essential oils in the nineteenth century, azulenic compounds continue to fascinate scientists to this day. The correct structure of the polar azulenic scaffold,  $C_{10}H_8$ , ( $\mu \approx 1.1$  Debye<sup>1</sup>) that features fused five- and seven-membered  $sp^2$ -carbon rings was first recognized by Pfau and Plattner in 1936.<sup>2</sup> The X-ray crystallographic confirmation of azulene's molecular structure was reported 20 years later.<sup>3,4</sup> Azulenic building blocks are attractive for developing  $\pi$ -functional molecules and materials.<sup>5–7</sup> Among the three possible linear biazulenes, 6,6'-biazulene has recently been emerging as a particularly effective oligoazulenic  $\pi$ -linker in the design of molecular electron reservoirs,<sup>8</sup> on-chip microsupercapacitors,<sup>9</sup> quasi-molecular rectifiers,<sup>10</sup> organic and organometallic self-assembled monolayer (SAM) films,<sup>8,11</sup> and organic field-effect transistors.<sup>12</sup> Since the synthesis of 6,6'-biazulene in 1980,<sup>13</sup> access to its derivatives, especially those functionalized along its molecular axis, has been quite limited.<sup>11,14,15</sup>

Given that azulene's highest occupied and lowest unoccupied molecular orbitals (HOMO/LUMO) have complementary orbital density distributions, their energies can be varied independently, to a first approximation.<sup>16–18</sup> This is accomplished by considering the position of attachment of a substituent to the azulenic core, as well as its electron withdrawing/donating ability.<sup>19</sup> In this communication, we envisioned a similar approach for tailoring the energetics of the frontier molecular orbitals of the linear 6,6'-biazulenic framework. Indeed, Fig. 1 illustrates the orbital density complementarity between the HOMO and LUMO of 6,6'-biazulene.

Herein, we demonstrate that the redox potential ( $E_{1/2}$ ) of the 6,6'-biazulenic scaffold is accurately predictable based on the Hammett  $\sigma_p$  parameters<sup>20</sup> of the substituents X and X' incorporated along its molecular axis (Fig. 2). To the best of our knowledge, this is the first study unveiling such quantitative redox correlations in the context of azulenic  $\pi$ -systems. In addition, we discuss how dichloro substitution exerts unexpected structural permutations within compound **3a** (X = X' = Cl) in the solid state.

To facilitate synthetic accessibility of 2,2'-functionalized 6,6'-biazulenes, we selected the 1,1',3,3'-tetraethoxycarbonyl-6,6'-biazulene (**1**) as the “parent” platform. Rather than employing a toxic organotin reagent to assemble **1** via Stille cross-coupling,<sup>21</sup> our synthesis of this compound involved simple deamination of the biazulenic derivative **2a** (Scheme 1). On the other hand, subjecting **2a** to Sandmeyer chlorination afforded dark purple, nearly black, crystalline

<sup>a</sup> Department of Chemistry, University of Kansas, Lawrence, KS 66045, USA.  
E-mail: mbarybin@ku.edu

<sup>b</sup> Department of Chemistry and Biochemistry, St. Catherine University, St. Paul, MN 55105, USA

<sup>c</sup> NMR Laboratory, Molecular Structures Group, University of Kansas, Lawrence, KS 66047, USA

<sup>†</sup> Electronic supplementary information (ESI) available: Experimental procedures, spectroscopic and analytical data, details of the electrochemical, X-ray crystallographic and DFT studies. CCDC 2300779. For ESI and crystallographic data in CIF or other electronic format see DOI: <https://doi.org/10.1039/d4cc00656a>

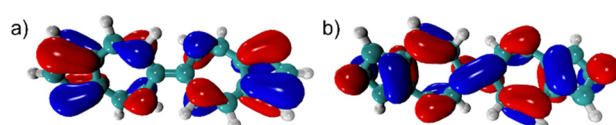


Fig. 1 Highest occupied (a) and lowest unoccupied (b) molecular orbitals (HOMO and LUMO) of 6,6'-biazulene (B3LYP functional and cc-pVQZ basis set).

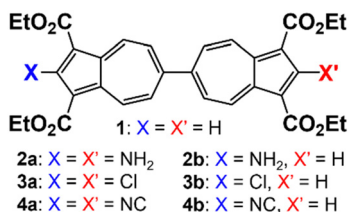
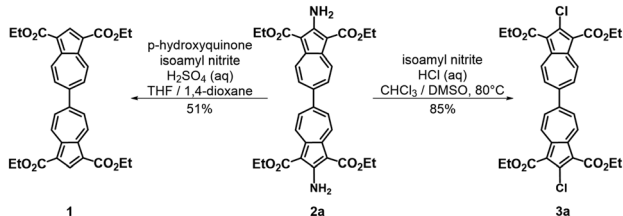


Fig. 2 2,2'-Functionalized 6,6'-biazulenes considered in this work.

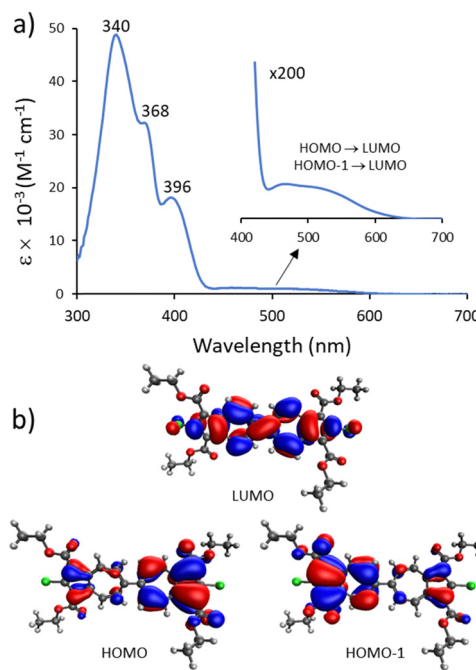
Scheme 1 Syntheses of 1,1',3,3'-tetraethoxycarbonyl-6,6'-biazulene (**1**) and 2,2'-dichloro-1,1',3,3'-tetraethoxycarbonyl-6,6'-biazulene (**3a**).

2,2'-dichloro-1,1',3,3'-tetraethoxycarbonyl-6,6'-biazulene (**3a**) in an 85% yield (Scheme 1). Thus, **3a** can be prepared from 2-amino-6-bromo-1,3-diethoxycarbonylazulene<sup>22</sup> in two steps with an overall yield of *ca.* 80% (Scheme S1, ESI†).<sup>14</sup> In addition to **3a**, we synthesized its unsymmetric congeners, 2-chloro-1,1',3,3'-tetraethoxycarbonyl-6,6'-biazulene (**3b**), *via* Sandmeyer chlorination of our recently reported 2-amino-1,1',3,3'-tetraethoxycarbonyl-6,6'-biazulene (**2b**) (Scheme 2).<sup>8</sup> Both **3a** and **3b** constitute versatile precursors to a variety of 2-, and 2,2'-functionalized 6,6'-biazulenes.

Given that unsymmetrically functionalized **3b** is a structural hybrid of centrosymmetric **1** and **3a**, it is reasonable that its <sup>1</sup>H NMR spectrum (Fig. S7, ESI†) appears as a superposition of the <sup>1</sup>H patterns observed for the latter compounds (Fig. S1 and S2, ESI†).

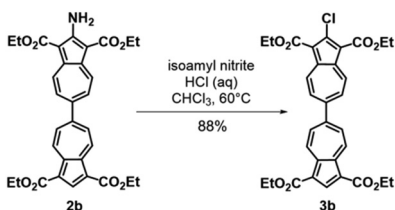
We assigned all resonances in the <sup>13</sup>C NMR spectrum of **3a** *via* synergistic consideration of its HSQC, HMBC, and 1,1-ADEQUATE<sup>23–26</sup> 2-D maps (Fig. S3–S6, ESI†). Notably, this is the only unambiguously assigned <sup>13</sup>C NMR profile of any 6,6'-biazulene reported in the literature to date.

Our TD-DFT calculations (Table S4, ESI†) corroborate that the lowest energy broad band centered around 500 nm in the electronic absorption spectrum of **3a** (Fig. 3a) corresponds to the HOMO → LUMO and HOMO-1 → LUMO transitions. The broad nature of this band can be attributed, in part, to the range of accessible microstates pertaining to the

Fig. 3 (a) Electronic absorbance spectrum of **3a** in  $CH_2Cl_2$  at  $22^\circ C$ . (b) TD-DFT calculated molecular orbitals of **3a** involved in the  $S_0 \rightarrow S_1$  transition.

azulene-azulene interplanar angle within **3a** in  $CH_2Cl_2$  solution.<sup>11</sup> While the LUMO of **3a** involves the entire biazulenic core, **3a**'s nearly degenerate HOMO and HOMO-1 are each primarily localized on one of the azulenic units (Fig. 3b).

We have recently shown that 2,2'-functionalized 6,6'-biazulenes undergo reversible one-step,  $2e^-$  reduction in  $CH_2Cl_2/n\text{-}Bu_4N^+\text{PF}_6^-$  solutions under the potential inversion regime<sup>27</sup> regardless of whether they feature symmetric or asymmetric substitution along their molecular axis.<sup>8</sup> After recognizing a qualitative relationship between the  $E_{1/2}$  values associated with the  $2e^-$  reduction of the 6,6'-biazulenic core and the electron donating/withdrawing characteristics of the 2,2'-substituents, we set out to identify a quantitative approach for tuning the 6,6'-biazulenic redox profile (Fig. S13–S16, ESI†). Remarkably, plotting the half-wave redox potential ( $E_{1/2}$ ) against the combined  $\sigma_p$  Hammett parameters<sup>20</sup> of the substituents X and X' for the seven 6,6'-biazulenic derivatives listed in Fig. 2 revealed a nearly perfect linear correlation over  $>600$  mV range (Fig. 4 and Table S5, ESI†). While attempts to correlate molecular redox potentials with the Hammett parameters of functional groups have been reported in the past for benzenoid organic/organometallic and ferrocene-based compounds,<sup>28–31</sup> this is the first example of invoking such a relationship for a cohort of azulenic derivatives. Notably, a similar trend ( $E_{p,c}$  vs.  $\sigma_p$ ) holds for the family of 2-substituted 1,3-diethoxycarbonyl azulenes shown in Fig. 5 and Table S6 (ESI†). However, the  $1e^-$  reduction of the latter compounds is invariably irreversible (Fig. S17–S20, ESI†).<sup>11</sup> Coupling any pair of 2-substituted azulenes to form the corresponding 6,6'-biazulene leads to full reversibility of the reduction, with the biazulenic  $E_{p,c}$

Scheme 2 Synthesis of 2-chloro-1,1',3,3'-tetraethoxycarbonyl-6,6'-biazulene (**3b**).

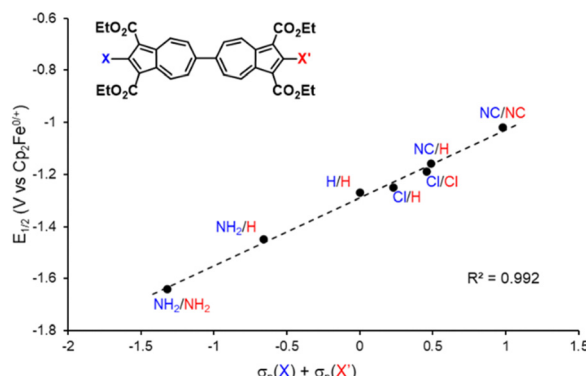


Fig. 4 A plot of the  $2e^-$  reduction potential ( $E_{1/2}$ ) for 2,2'-functionalized 6,6'-biazulenes vs. the combined  $\sigma_p$  Hammett parameters of the substituents X and X'.

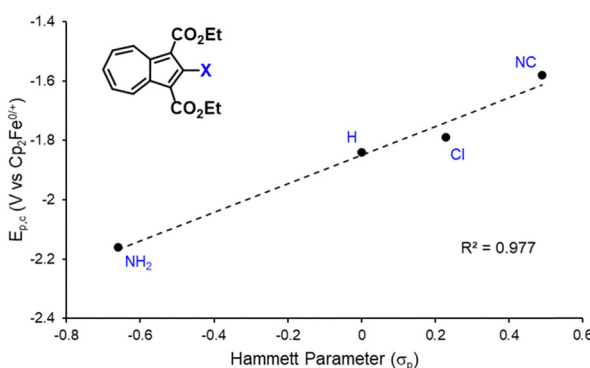


Fig. 5 A plot of the reduction potential ( $E_{pc}$ ) for 2-functionalized 1,3-diethoxycarbonylazulenes vs. the  $\sigma_p$  Hammett parameter of the substituent X.

being  $0.51 \pm 0.04$  V more positive compared to the average  $E_{pc}$  of the monoazulenes (Tables S5 and S6, ESI<sup>†</sup>). This is a consequence of the substantially greater resonance stabilization energy of the 6,6'-biazulenic framework.

The molecular structure of **3a** is illustrated in Fig. 6. The two chemically identical, but crystallographically unique C–Cl bonds, C2–Cl1 and C2'–Cl2, within **3a** have the lengths of 1.674(2) Å and 1.682(2) Å, respectively. The longer C–Cl bond

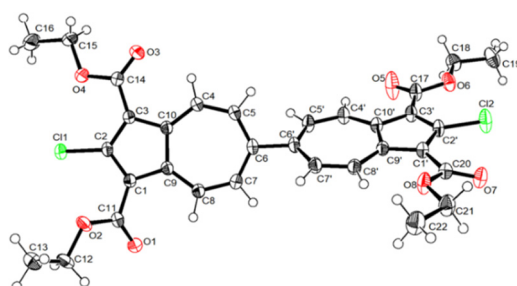


Fig. 6 Molecular structure of **3a** (50% thermal ellipsoids). Selected interatomic distances (Å) and dihedral angle (deg): C2–Cl1 1.674(2), C2'–Cl2 1.682(2), C6–C6' 1.478(2), C9–C10 1.437(2), C9'–C10' 1.440(3), O2..Cl1 2.918(2), O4..Cl1 2.834(1), O6..Cl2 2.816(2), O7..Cl2 2.876(2), C5–C6–C6'–C5' 48.1(2).

Table 1 Comparison of C(2)–Cl and C(9)–C(10) bond distances in X-ray structurally characterized 2-chloroazulenic derivatives

Compound	$d(\text{C}^2\text{--Cl})$ Å	$d(\text{C}^9\text{--C}^{10})$ Å	CCDC identifier
	1.674(2) 1.682(2)	1.437(2) 1.440(3)	This work
	1.712(2)	1.471(2)	HOMRAE
	1.714(4)	1.470(6)	XIGPOU
	1.709(2)	1.470(3)	AYIDIX

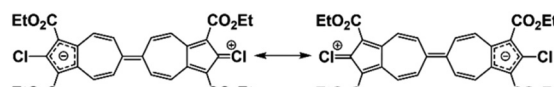


Fig. 7 Minor zwitterionic resonance forms of **3a**.

belongs to the half of the molecule featuring the shortest Cl···O contact (Cl2···O6) of 2.816 Å. Both C–Cl bonds in **3a** are significantly shorter than any C–Cl bond in all structurally characterized chloroazulenes featuring Cl-substitution at the five-membered ring of the azulenic scaffold (Fig. S22 and Table S14, ESI<sup>†</sup>). In particular, the C–Cl bonds in **3a** are statistically shorter, per the 3- $\sigma$  criterion,<sup>32</sup> than those in the X-ray structures of the other three 2-chloroazulenes known to date (Table 1).<sup>33–35</sup>

The C–Cl bond contractions in **3a** may be rationalized by invoking the minor heptafulvalene-like zwitterionic resonance forms depicted in Fig. 7, which show C=Cl double-bond character. This argument mirrors the crystallographic analysis of the chlorodiphenylmethyl cation by Laub *et al.*<sup>36</sup> The short C–Cl bond distance of 1.668(8) Å within this carbocation, which is statistically indistinguishable from those in **3a**, was attributed to chlorine back-donation exerting partial double-bond C=Cl<sup>+</sup> character (Fig. S23, ESI<sup>†</sup>).<sup>36</sup> Unusually short C–Cl bonds, including various C–Cl multiple bonding scenarios, continue to attract both experimental and theoretical interest.<sup>37–39</sup>

The C6–C6' bond distance of 1.478(2) Å within **3a** is markedly shorter than those in all other crystallographically characterized 6,6'-biazulenes (Table 2).<sup>8,11,12,40</sup> In addition, as summarized in Table 2, the C–C bonds at the fusion of the five- and seven-membered rings in **3a** are substantially contracted as well. Both of these observations are consistent with a nontrivial heptafulvalene-like contribution to the structure of the biazulenic scaffold of **3a**.<sup>41</sup> Moreover, the azulene–azulene interplanar angles in dichloro **3a** and diisocyano **4a**, which share the same 1,1',3'3'-tetraethoxycarbonyl-6,6'-biazulenic core, are 48.1° and 66.9°,<sup>11</sup> respectively, although such comparison should be viewed *cum grano salis* as this torsion parameter is undoubtedly sensitive to crystal packing.

In summary, we demonstrated that the redox profile of the 6,6'-biazulenic scaffold functionalized along its molecular axis is quantitatively tuneable within a wide window of potentials.

**Table 2** Comparison of C(6)–C(6') and C(9)–C(10) bond distances in X-ray structurally characterized 6,6'-biazulenes

Compound	$d(\text{C}^6-\text{C}^{6'})$ , Å	$d(\text{C}^9-\text{C}^{10})$ , Å	CCDC identifier
	1.478(2)	1.437(2) 1.440(3)	This work
	1.498(2)	1.485(2) 1.488(2)	NAZROZ
	1.512(4)	1.475(3)	OSIGED
	1.497(3) 1.499(3)	1.465(3)–1.476(3)	HITRIP <sup>a</sup>

<sup>a</sup> Two crystallographically independent molecules in the asymmetric unit.

This was accomplished by considering, for the first time in the context of azulenic systems, the well documented  $\sigma_p$  Hammett parameters<sup>20</sup> reflecting the net electronic influence of the substituents. We anticipate that the facile access to the crystallographically unusual dichloro derivative **3a** offers not only new opportunities to engage the 6,6' architecture as an attractive molecular template in the realm of organic charge transfer and/or conductive materials, but also to explore unorthodox approaches for pursuing C–Cl multiple bonding.

This research was funded by the US National Science Foundation grant CHE-1808120 to M. V. B. S. R. K. acknowledges the support provided by the NSF Graduate Research Fellowship under grant DGE-1940699 and the Madison and Lila Self Graduate Fellowship at the University of Kansas. Support for the NMR instrumentation was provided by NIH Shared Instrumentation Grants (S10OD016360 and S10RR024664), NSF MRI funding (CHE-1625923 and CHE-9977422), and an NIH Center Grant (P20 GM103418). The calculations were performed at the University of Kansas Center for Research Computing (CRC), including the BigJay cluster resource funded through NSF Grant No. MRI-2117449. X-ray crystallographic resources were provided by an NSF-MRI award #1125975. This manuscript is dedicated to Prof. John E. Ellis of the University of Minnesota.

## Conflicts of interest

There are no conflicts to declare.

## Notes and references

1. A. G. Anderson and B. M. Steckler, *J. Am. Chem. Soc.*, 1959, **81**, 4941–4946.
2. A. St. Pfau and P. A. Plattner, *Helv. Chim. Acta*, 1936, **19**, 858–879.
3. J. M. Robertson and H. M. M. Shearer, *Nature*, 1956, **177**, 885.
4. J. M. Robertson, H. M. M. Shearer, G. A. Sim and D. G. Watson, *Nature*, 1958, **177**–178.
5. H. Katagiri, in *Advances in Organic Crystal Chemistry*, ed. H. Uekusa and M. Sakamoto, Wiley, 2020, pp. 341–358.
6. J. Huang, S. Huang, Y. Zhao, B. Feng, K. Jiang, S. Sun, C. Ke, E. Kymakis and X. Zhuang, *Small Methods*, 2020, **4**, 2000628.
7. H. Xin, B. Hou and X. Gao, *Acc. Chem. Res.*, 2021, **54**, 1737–1753.
8. P. T. Connolly, J. C. Applegate, D. A. Maldonado, M. K. Okeowo, W. C. Henke, A. G. Oliver, C. L. Berrie and M. V. Barybin, *Dalton Trans.*, 2023, **52**, 11419–11426.

9. C. Yang, K. S. Schellhammer, F. Ortmann, S. Sun, R. Dong, M. Karakus, Z. Mics, M. Löffler, F. Zhang, X. Zhuang, E. Cánovas, G. Cuniberti, M. Bonn and X. Feng, *Angew. Chem., Int. Ed.*, 2017, **56**, 3920–3924.
10. S. Sun, X. Zhuang, L. Wang, B. Zhang, J. Ding, F. Zhang and Y. Chen, *J. Mater. Chem. C*, 2017, **5**, 2223–2229.
11. T. R. Maher, A. D. Spaeth, B. M. Neal, C. L. Berrie, W. H. Thompson, V. W. Day and M. V. Barybin, *J. Am. Chem. Soc.*, 2010, **132**, 15924–15926.
12. Y. Shibuya, K. Aonuma, T. Kimura, T. Kaneko, W. Fujiwara, Y. Yamaguchi, D. Kumaki, S. Tokito and H. Katagiri, *J. Phys. Chem. C*, 2020, **124**, 4738–4746.
13. M. Hanke and C. Jutz, *Synthesis*, 1980, 31–32, DOI: [10.1055/s-1980-28911](https://doi.org/10.1055/s-1980-28911).
14. An alternative synthesis of **3a** from 2-amino-6-bromo-1,3-dioxy carbonylazulene, albeit in a three-step sequence with an overall *ca.* 45% yield, has been recently reported: B. Hou, Z. Zhou, C. Yu, X. S. Xue, J. Zhang, X. Yang, J. Li, C. Ge, J. Wang and X. Gao, *ACS Macro Lett.*, 2022, **11**, 680–686.
15. Y. Yamaguchi, M. Takubo, K. Ogawa, K. Nakayama, T. Koganezawa and H. Katagiri, *J. Am. Chem. Soc.*, 2016, **138**, 11335–11343.
16. R. S. H. Liu and A. E. Asato, *J. Photochem. Photobiol. C*, 2003, **4**, 179–194.
17. R. S. H. Liu, *J. Chem. Ed.*, 2002, **79**, 183–185.
18. R. P. Steer, *J. Photochem. Photobiol. C*, 2019, **40**, 68–80.
19. R. E. Robinson, T. C. Holovics, S. F. Deplazes, D. R. Powell, G. H. Lushington, W. H. Thompson and M. V. Barybin, *Organometallics*, 2005, **24**, 2386–2397.
20. R. W. Taft, A. Leo and C. Hansch, *Chem. Rev.*, 1991, **91**, 165–195.
21. S. Ito, T. Okujima and N. Morita, *J. Chem. Soc., Perkin Trans. 1*, 2002, 1896–1905.
22. T. C. Holovics, R. E. Robinson, E. C. Weintrob, M. Toriyama, G. H. Lushington and M. V. Barybin, *J. Am. Chem. Soc.*, 2006, **128**, 2300–2309.
23. G. E. Martin, *Annual Reports on NMR Spectroscopy*, Elsevier, 2011, ch. 5, vol. 74, pp. 215–291.
24. B. D. Hilton, K. A. Blinov and G. E. Martin, *J. Nat. Prod.*, 2011, **74**, 2400–2407.
25. M. M. Senior, R. T. Williamson and G. E. Martin, *J. Nat. Prod.*, 2013, **76**, 2088–2093.
26. A. V. Buevich, R. T. Williamson and G. E. Martin, *J. Nat. Prod.*, 2014, **77**, 1942–1947.
27. D. H. Evans, *Chem. Rev.*, 2008, **108**, 2113–2144.
28. L. Wang, Z. L. Xie, B. T. Phelan, V. M. Lynch, L. X. Chen and K. L. Mulfort, *Inorg. Chem.*, 2023, **62**, 14368–14376.
29. J. C. Dickenson, M. E. Haley, J. T. Hyde, Z. M. Reid, T. J. Tarring, D. A. Iovan and D. P. Harrison, *Inorg. Chem.*, 2021, **60**, 9956–9969.
30. W. C. Henke, D. Lionetti, W. N. G. Moore, J. A. Hopkins, V. W. Day and J. D. Blakemore, *ChemSusChem*, 2017, **10**, 4589.
31. N. Vo, N. L. Haworth, A. M. Bond and L. L. Martin, *ChemElectroChem*, 2018, **5**, 1–14.
32. F. Pukelsheim, *Am. Stat.*, 1994, **48**, 88–91.
33. S. Förster, W. Seichter, R. Kuhnert and E. Weber, *J. Mol. Struc.*, 2014, **1075**, 63–70.
34. K. J. Scheetz, A. D. Spaeth, A. S. Vorushilov, D. R. Powell, V. W. Day and M. V. Barybin, *Chem. Sci.*, 2013, **4**, 4267–4272.
35. B. B. Ling, *CSD Commun.*, 2016, CCDC 888557, DOI: [10.5517/ccdc.csd.ccym4h](https://doi.org/10.5517/ccdc.csd.ccym4h).
36. T. Laube, E. Bannwart and S. Hollenstein, *J. Am. Chem. Soc.*, 1993, **115**, 1731–1733.
37. F. Fantuzzi, B. Rudek, W. Wolff and M. A. C. Nascimento, *J. Am. Chem. Soc.*, 2018, **140**, 4288–4292.
38. R. Kalesky, E. Kraka and D. Cremer, *Int. J. Quantum Chem.*, 2014, **114**, 1060–1072.
39. M. Göbel, B. H. Tchitchanov, J. S. Murray, P. Politzer and T. M. Klapotke, *Nat. Chem.*, 2009, **1**, 229–235.
40. Not included in Table 2 is the structure of 2,2'-dibromo-1,1'-dibutyl-6,6'-biazulene that is searchable in CCDC (NAPSUW) but suffers from low precision {e.g.,  $d(\text{C}^6-\text{C}^{6'}) = 1.50(2)$  Å}, unacceptable data/refinement quality ( $R$ -factor = 11.7%), and lack of a published synthesis: B. Hou, *CSD Commun.*, 2021, CCDC 2127392.
41. R. Thomas and P. Coppens, *Acta Crystallogr., Sect. B: Struct. Crystallogr. Cryst. Chem.*, 1972, **28**, 1800–1806.